Modeling excitonic line shapes in weakly disordered semiconductor nanostructures

I. Kuznetsova,[1] N. Gőgh,[2] J. Förstner,[1] T. Meier,[1] S. T. Cundiff,[3] I. Varga,[4] and P. Thomas[2]
[1]*Department Physik, Fakultät für Naturwissenschaften and CeOPP, Universität Paderborn, Warburger Strasse 100, D-33098 Paderborn, Germany*
[2]*Department of Physics and Material Sciences Center, Philipps University, Renthof 5, D-35032 Marburg, Germany*
[3]*JILA, University of Colorado and National Institute of Standards and Technology, Boulder, Colorado 80309-0440, USA*
[4]*Department of Theoretical Physics, Institute of Physics, Budapest University of Technology and Economics, Budafoki út 8. H1111 Budapest, Hungary*

(Received 12 October 2009; revised manuscript received 21 December 2009; published 8 February 2010)

Excitonic spectra of weakly disordered semiconductor heterostructures are simulated on the basis of a one-dimensional tight-binding model. The influence of the length scale of weak disorder in quantum wells on the redshift of the excitonic peak and its linewidth is studied. By calculating two-dimensional Fourier-transform spectra we are able to determine the contribution of disorder to inhomogeneous and also to homogeneous broadenings separately. This disorder-induced dephasing is related to a Fano-type coupling and leads to contributions to the homogeneous linewidth that depends on energy within the inhomogeneously broadened line. The model includes heavy- and light-hole excitons and yields smaller inhomogeneous broadening for the light-hole exciton if compared to the heavy-hole exciton, which agrees qualitatively with the experiment.

DOI: 10.1103/PhysRevB.81.075307 PACS number(s): 78.67.−n, 71.23.An, 78.47.nj, 42.50.Md

I. INTRODUCTION

Semiconductor heterostructures generally possess a certain degree of disorder. In a quantum well, e.g., it results from either static fluctuations of the well width or from alloy disorder. The electronic and optical properties of these structures are sensitive to disorder and it is desirable to determine to what extent these properties are influenced by the parameters characterizing a given type of disorder. In this work we study the impact of weak disorder on linear and nonlinear optical excitonic spectra in model calculations.

The theoretical treatment of disorder and many-body interactions on an equal footing is still a demanding task. There are various ways to solve this problem. Assuming that the optical properties being studied are self-averaging, one can set up the set of equations of motion for the relevant dynamical variables, which in this case are the configurationally averaged linear and nonlinear optical polarizations. This scheme requires an approximation to obtain a closed set of equations.[1] It has been shown, however,[2] that, in particular, the second Born approximation is ill controlled and leads to unphysical results.

Alternatively, one calculates the dynamical variables for given realizations of disorder and averages at the end. Approximations are thus avoided and the model is evaluated in a numerically exact way. For the calculation of linear spectra, direct diagonalization of the Hamiltonian with subsequent averaging is also possible. In the present work we will follow this approach.

While certain aspects of disorder-induced features of linear spectra have been studied by analytical and numerical approaches, the majority of model calculations, in particular, for nonlinear optical properties, have been performed using a one-dimensional tight-binding model,[3] which in a real-space basis allows one to include disorder in a natural way.

Previous studies include the calculation of linear absorption spectra,[4–8] pump-probe spectra,[9] time-resolved and time-integrated four-wave-mixing (FWM) traces,[10–12] and two-dimensional Fourier-transform spectra [2DFTS, a variant of FWM (Ref. 13)].[14] In linear spectra, the inhomogeneous linewidth and the asymmetry of excitonic spectra have been related to disorder parameters such as amplitude and length scale.[6] On the other hand, nonlinear optical spectroscopies allow one to separate homogeneous (optical dephasing) and inhomogeneous contributions to the excitonic linewidth. In calculations of FWM traces for relatively large disorder, it has been shown that disorder not only results in echoes but also contributes to dephasing ("disorder-induced dephasing").[10–12,15] For weak disorder, compared to time-resolved and time-integrated FWM traces, the 2DFTS scheme has advantages for the study of contributions to the excitonic linewidth.[16] However, the results obtained so far are not based on a microscopic implementation of the disorder potential, such that disorder-induced dephasing could not be studied in Ref. 16. By a convolution of spectra determined for ordered models with a Gaussian distribution of gap energies it was illustrated how one can determine homogeneous and inhomogeneous contributions to the linewidth for cases where disorder is weak and where more than just a single excitonic transition exists.

Since the calculations aim at experimentally accessible data which are first (linear) or third order (FWM) in the excitation light field, the Coulomb interaction can be treated in the Hartree-Fock (HF) or beyond HF limit, i.e., including coherent biexcitonic (many-particle) correlations.[15] For the determination of the optical properties in these schemes, the semiconductor Bloch equations need to be solved numerically for the optical polarization in the required order in the external light field.

Following this approach, we are able to identify microscopic mechanisms that lead to disorder-induced features of the excitonic spectra. In particular, we concentrate on disorder resulting from local fluctuations of the confinement potential, giving rise to a weak (with respect to the exciton binding energy) correlated disorder potential for electrons

and holes. It is furthermore characterized by a certain length scale.

We start by studying in detail the influence of the length scale of the disorder potential on linear spectra and demonstrate the interplay of Coulomb and disorder effects that leads to universal behavior in the regime where length scale is smaller than excitonic Bohr radius. Then, based on the discussion of 2DFTS, a deeper understanding of the previously introduced notion of disorder-induced dephasing is achieved by noting two facts. (i) excitonic transitions in a disordered low-dimensional (here one-dimensional) environment are spatially localized with respect to their center-of-mass (COM) motion and (ii) due to the nonperiodic potential causing a violation of the selection rule for the COM momentum, it couples to the light field. In addition the COM continuum will be modified due to localization.[6] This coupling leads to a scenario known as Fano coupling[17,18] that contributes to the homogeneous linewidth.

This paper is organized as follows: in Secs. II and III we set up the tight-binding model, implement the disorder potential characteristic for well-width fluctuations, and briefly discuss the solution of the equation of motion for the linear and nonlinear optical polarizations. In Sec. IV the linear spectra are studied as a function of the length scale of the disorder potential. In Sec. V 2DFTS are discussed for a simple Fano situation and an application to excitonic spectra is discussed. In Sec. VI calculations of 2DFTS are shown for the semiconductor model and analyzed in order to identify homogeneous and inhomogeneous broadening of the transitions separately. In the concluding Sec. VII we discuss the good qualitative agreement that is obtained from the comparison of our simulations with experimental data.

II. MODEL

Instead of intending to model a given semiconductor heterostructure, in this work we study disorder-induced features and mechanisms for a model system that on one hand, comprises the relevant features determining the optical response of realistic heterostructures and on the other hand, is numerically tractable. This model is then evaluated without using any approximation. Limitations are then only due to model assumptions. Indeed our model is not intended to yield quantitative agreement with experimental data obtained on three-dimensional quantum structures. However, a large body of experience (see, e.g., Refs. 10–12, 14, and 19, and, in particular, Ref. 15 and references therein) with this model has shown that general trends in optical data as a function of physical parameters and also microscopic mechanisms underlying these trends can clearly be identified using this approach.

We use a one-dimensional two-band tight-binding model, for details see Refs. 10 and 15. It consists of a periodic chain of sites with nearest-neighbor separation a and periodic boundary conditions. Each site i carries a single electron level ϵ_i^c and one or two hole levels ϵ_i^v, where v denotes a heavy-hole (h) or light-hole (l) state. The states of nearest-neighbor sites i,j are coupled by matrix elements J^λ, where $\lambda=c,h,l$. This model is characterized by single-particle cosine bands, which in the vicinity of the direct gap are parabolic. The model parameters a and J^λ determine the effective masses via $m^\lambda=\hbar^2/(2|J^\lambda|a^2)$. Other parameters of the model are listed below. N is the number of sites, μ^v are the optical dipole elements for transitions between hole band v and electron band c. V_0 is the parameter determining the strength of the Coulomb interaction, which together with a regularization parameter $a_0=0.5a$ determines the exciton binding energies and, together with the masses, also the exciton Bohr radius a_B. This parameter is a necessary requisite in one-dimensional models which removes the unphysical divergence of the exciton binding energy.[20] T_2^v are phenomenological dephasing times. The excitation pulses are taken to have Gaussian envelope with time scale of 100 fs and central frequency close to the excitonic resonances. M is the number of realizations of the disorder potential. W^λ is the width of the boxlike distribution of site energies around zero mean. L denotes the length scale of the disorder potential. As the value of a is determined by the masses m^λ and the J^λ but otherwise does not appear in the results, we normalize all lengths with respect to a. For our choice of J^λ and the strength of the Coulomb potential V_0, the exciton Bohr radius a_B is about two times a and its binding energy is sufficiently larger than the exciton linewidth.

Henceforth in this paper, we model correlated disorder, which reflects the fact that a decrease in the width of the quantum well causes the electron and heavy- and light-hole valence-band energies shift to opposite directions, thereby producing larger gaps between the c and v levels at a given site. In this scenario, the widths of the box distributions W^λ scale with the inverse masses of the particles, which are inversely proportional to J^λ. Thus the relevant dimensionless disorder parameter is the ratio W/J.

The length scale L is implemented as follows. For a given realization the site energies are drawn from the box-distribution resulting in a discrete function ϵ_i (we omit the upper index λ for clarity here). The standard deviation is determined. Then $\hat{\epsilon}(k)$, the Fourier transform of ϵ_i is multiplied with a Gaussian $\propto\exp(-L^2k^2/4)$ and back transformed into site representation. The resulting potential has smaller standard deviations than the original one, see Fig. 1. Therefore it is renormalized such that its standard deviation agrees with the original one. In the inset of Fig. 1, the spatial high-frequency components are thus removed in a disorder potential with larger length scale.

In Sec. VI we will choose the model parameters having GaAs/AlGaAs quantum wells in mind. Application of 2DFTS for the ordered situation has been discussed in Ref. 14. There the effective mass of the heavy hole has been taken to be larger than that for the light hole. Thus, in the present context, the amplitude of the disorder potential of the light-hole states is larger than that of the heavy-hole states.

III. THEORETICAL METHOD

In this work, we consider linear and nonlinear optical spectra that are experimentally determined by applying short (typically 100 fs) pulses to the sample. The temporal response, given by the optical polarization P, is then Fourier

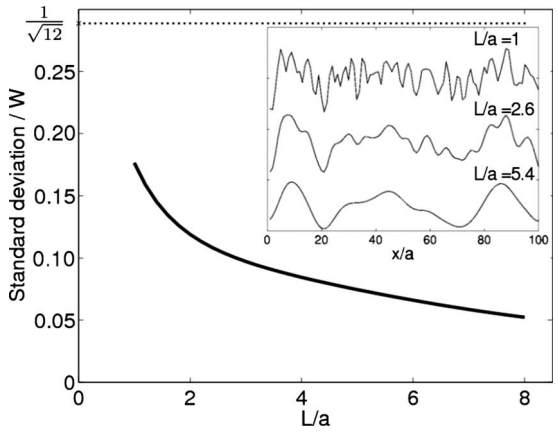

FIG. 1. Dependence of the standard deviation of the disorder potential on the length scale L/a before renormalization. The horizontal line indicates the standard deviation of the potential resulting from the original box distribution. Inset: representation of the renormalized disorder potentials for different length scale.

transformed with respect to real time by the spectrometer and, in the case of 2DFTS, also numerically with respect to time delay between excitation pulses.[21] Theoretically, we follow this scheme and calculate P in the time domain from the equation of motion that include the pulse excitation as given by the experiment.[15,19] For an alternative theoretical treatment of 2DFTS see Refs. 22 and 23. In the case of linear spectra we also use direct diagonalization and the Elliott formula.[24]

The optical polarization P is given by the microscopic polarization $p_{ij}=\langle v_i^{h,l} c_j \rangle$, where v_i and c_j (h,l) are hole and electron operators, respectively.[15] This time-dependent function is calculated for each of the M different realizations of the disorder potential. The ensemble averaged polarization is then determined by superposition.

In short-hand notation (for the full expressions see, e.g., Refs. 9, 10, and 15), the equation of motion for the linear polarization $(\chi^{(1)})$ reads

$$-i\hbar\frac{d}{dt}p = -\hbar\omega_x p + \mu^* E, \tag{1}$$

where ω_x is the single-particle Hamiltonian matrix including the electron-hole attraction, the site energies, and the intersite couplings. E is the pulsed electric laser-light field. Multiplying the resulting p by μ and summing over all sites yields P. This function is then Fourier transformed, its imaginary part is the linear absorption spectrum.

The two-dimensional nonlinear spectra display the electric field $E(\omega_t,\omega_\tau,T)$. It is proportional to the Fourier transform of the nonlinear optical polarization $P(t,\tau,T)$. Here t is the time, τ the delay between first and second excitation pulses, and T that between second and third pulses. We take $T=100$ fs throughout. The frequency variables ω_t and ω_τ refer to the time variables t and τ, respectively. Since $E(\omega_t,\omega_\tau,T)$ is a complex-valued function, we can plot its real part, imaginary part, and amplitude. In this work we only consider the so-called rephasing mode, where the first two pulses are arranged in time such that a photon echo would result in the temporal response. Conventionally, the spectra are then plotted for positive ω_t and negative ω_τ, such that the diagonal $\omega_t=-\omega_\tau$ extends from the upper-left to the lower-right corner of the two-dimensional plot. (For clarity, in this work, we indicate the energies only at the horizontal ω_t axis, the energies at the $-\omega_\tau$ axis follow from reflection at the diagonal.)

In the above short-hand notation, the equation of motion for the nonlinear $(\chi^{(3)})$ microscopic polarization reads

$$-i\hbar\frac{d}{dt}p = -\hbar\omega_x p + Vp^*pp + V\bar{B}p^* + \mu^* E - \mu^* E p^* p, \tag{2}$$

where $\bar{B}$ describes the biexciton many-particle correlations beyond HF and obeys the equation of motion

$$-i\hbar\frac{d}{dt}\bar{B} = -\hbar\omega_{2x}\bar{B} + Vpp. \tag{3}$$

Here ω_{2x} is the two-particle Hamiltonian matrix containing also all two-particle Coulomb interactions between the two electrons and two holes. This closed set of equations follows from the dynamics-controlled truncation scheme,[15,25] which is the consistent treatment of the Coulomb interaction for $\chi^{(3)}$ processes like FWM and 2DFTS.

Disorder and many-particle interaction both lead to spectral features that are not easy to disentangle. Therefore, we will also use calculations where certain aspects of the Coulomb interaction are omitted. In particular, we may write (again in short-hand notation)[9]

$$P = P_{pb} + P_{1\mathrm{st}} + P_{corr}. \tag{4}$$

Here P_{pb} refers to the Pauli-blocking limit, which results from Eq. (2) if the second and third terms on the right-hand side are omitted. $P_{pb}+P_{1\mathrm{st}}$ denotes the HF limit, where only the third term is omitted. $P=P_{pb}+P_{1\mathrm{st}}+P_{corr}$ is the full result including the many-particle correlations.

IV. LINEAR SPECTRA

In this section we focus on a single excitonic line. Prior work has shown that disorder leads to various effects including a redshift of the excitonic peak relative to ordered case, an asymmetric line shape and broadening of the line.[6,7] Even in an ordered situation the excitonic line shape is not symmetric, which is due to the electron-phonon interaction.[26,27] This effect will not be treated in this work, assuming that disorder effects dominate the line shape. However, an asymmetric line shape in the ordered case is also due to the coupling between exciton and the pair continuum, which is included in our calculations. This coupling depends on the excitonic binding energy, for smaller binding energy we observe a more asymmetrical absorption line. Therefore, for larger binding energy (about 19 meV) in the ordered situation we have an almost symmetric Lorentzian due to phenomenological dephasing. It is assumed that disorder effects dominate the line shape of the disordered situation.

A. Dependence of linewidth on disorder length scale

Disorder broadens the absorption line. It is known[5] that alloy disorder has a different impact on the line shape com-

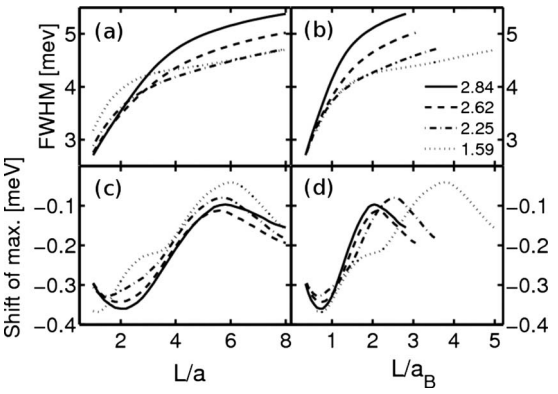

FIG. 2. Upper row: FWHM of the absorption spectra of the exciton and lower row: shift of the maximum of the excitonic absorption line. Left-hand column: plotted vs L/a and right-hand column: plotted vs L/a_B. Various curves refer to a_B/a as given in (b). Disorder parameter is $W/J=0.2$.

pared to interface roughness. In this work, we consider interface roughness as the dominant source of disorder in a semiconductor quantum structure.

The linear spectra have been calculated using direct diagonalization and the Elliott formula.[24] We have also used the equation of motion approach with very short excitation pulses solved in the linear regime. The results agree perfectly, however, the former approach is by far numerically faster.

The features of the inhomogeneously broadened lines depend on the interplay of disorder and Coulomb effects. Both of them are characterized by a length scale. The disorder potential is characterized by L/a while the Coulomb effects reflect the excitonic Bohr radius a_B/a.[28] In order to clearly identify the Coulomb-related features width (the full width at half maximum, FWHM) and shift are plotted not only as a function of L/a but also against L/a_B, see Figs. 2(a), 2(c), 2(b), and 2(d), respectively.

For the length scale smaller than Bohr radius it is known[4,7] that the exciton relative motion averages over the disorder potential resulting in a reduced amplitude of the effective potential and an effective length scale close to the Bohr radius. This reduced disorder strength leads to a reduced inhomogeneous width. For a length scale L much larger than the Bohr radius the Bohr radius does not directly influence the spectral width. For large L one expects a saturation value of the width. See Fig. 2(a), which shows the increase in the FWHM with L for different strength of the Coulomb interaction. The strength of the Coulomb interaction is here given by the corresponding Bohr radius [see labels on Fig. 2(b)]. In Fig. 2(a) we notice that the width increases with disorder length scale monotonically. However, for different Coulomb strength, as quantified by the legend given in Fig. 2(b), there is no universal behavior.

On the other hand, if we plot the FWHM width versus L scaled by the Bohr radius, a clear trend can be seen [Fig. 2(b)]. For the length scale less than the Bohr radius a seemingly universal behavior results, indicating that the spectra are indeed determined by the ratio of the length scale and the Bohr radius. For larger length scale a universal behavior is seen more clearly in Fig. 2(a), indicating that here the role of the Coulomb effects is less dominant.

These curves do not approach a single value for large L. This divergence is due to the electron-hole pair continuum which contributes to the width, in particular, for small binding energy.

The lower part of the figure shows the shift of the excitonic peak relative to the one in ordered case [Figs. 2(c) and 2(d)]. Here it is important to remark that the energy scale of this shift is much less than FWHM. Obviously, the dependence of the shift on length scale is nonmonotonic. Again we see different regimes. For the length scale less than the Bohr radius Fig. 2(d) indicates that there is a universal character (the shift becomes larger), determined only by the ratio of length scale and Bohr radius. On the other hand, for increasing length scales beyond Bohr radius, the excitonic peak moves toward higher energy and finally returns back to the lower energy. The Bohr radius no longer influences the shift directly. This turning back of the peak toward lower energy for large and increasing L is not physical but is an effect of the finite size of our model.

Thus both width and shift are determined by L/a_B, if $L < a_B$ in a universal manner. For larger L the Coulomb interaction does not directly influence the dependence of the spectral features on L.

B. Dependence of linewidth on hole mass

Existing experiments[14,29] indicate that the inhomogeneous width of the light-hole exciton is smaller than that of the heavy-hole exciton. In this section we, also for later reference, study the effect of hole mass on the width of the linear spectrum. The mass of electron and/or hole influences the inhomogeneous width via two different mechanisms. In the present model of disorder due to well-width fluctuations, the variance of the disorder potential for a particular particle increases linearly with its reciprocal mass, i.e., with its coupling J. On the other hand, for decreasing reduced excitonic mass, being $\propto 1/(|J^c|+|J^v|)$, the Bohr radius a_B increases and thus the averaging effect becomes more pronounced. Figure 3 demonstrates the crossover between these two regimes.

In this figure we display the dependence of the FWHM of exciton absorption spectra on coupling parameter J^v, i.e., on effective hole mass. The disorder parameter W/J was kept constant. We expect that the increasing the coupling parameter J^v increases the width via increasing disorder amplitude. This expectation is true for $J^v > 1.5$ meV. For the small coupling parameter J^v we observe a decrease in the FWHM with increasing of coupling parameter J^v. Here the averaging effect dominates over the above-mentioned mechanism. See Fig. 1, where the standard deviation of the unrenormalized potential is shown as a function of its length scale. In the present context the length scale should be identified with a_B, which increases with J^v. The initial strong drop of the standard deviation with L (a_B) is the reason for the initial drop of the FWHM in Fig. 3. It is therefore clear that a universal monotonic dependence of inhomogeneous width on mass of the particles does not exist.

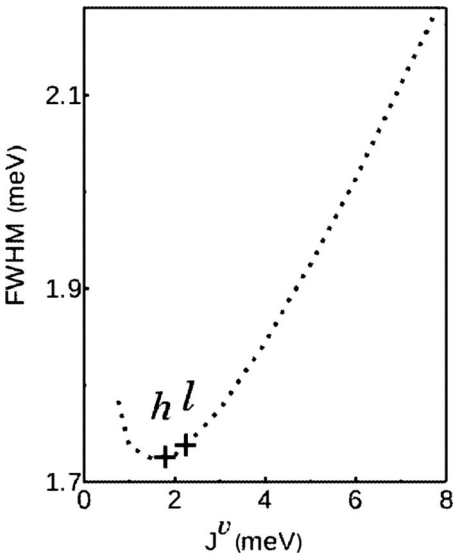

FIG. 3. FWHM extracted from the linear spectra of the excitonic line for $N=100$ and the number of realizations $M=100$ and $W/J=0.4$. Disorder length scale is $L=a$. Crosses depict values for J^v of 1.8 and 2.25 meV, which we will discuss in Sec. VI.

V. TWO-DIMENSIONAL FOURIER-TRANSFORM SPECTROSCOPY

In the second part of the paper we take advantage of the recently developed technique of two-dimensional Fourier-transform spectroscopy,[30] applied to semiconductors. One of the applications of this experiment is to identify the homogeneous and inhomogeneous contributions of the broadenings to the linewidth of the exciton. In this variant of a FWM experiment the temporal order of the first two excitation pulses can be interchanged, leading to the rephasing and nonrephasing modes. Using these two operating modes, we are able to resolve the spectra and define those broadenings for each spectral contribution separately.[16] In the following 2DFTS, the vertical scale follows from the horizontal one by mirror reflection at the diagonal. In this work we will consider cocircularly polarized excitation pulses exclusively. In this case contributions due to bound biexcitons are absent. Biexcitons would obscure the disorder-induced features in the spectra for weak disorder.

A. Fano features

In the following section, we consider the influence of coupling to continuum states on homogeneous broadening. Optical transitions between discrete states that are coupled to transitions into a continuum are known to result in asymmetrical line shapes in the linear optical spectrum.[17,18] This so-called Fano situation can also be identified applying two-dimensional Fourier-transform spectroscopy. We will demonstrate that due to the Fano effect, disorder contributes to the homogeneous linewidth of the exciton.

In the typical Fano situation there is an optical transition

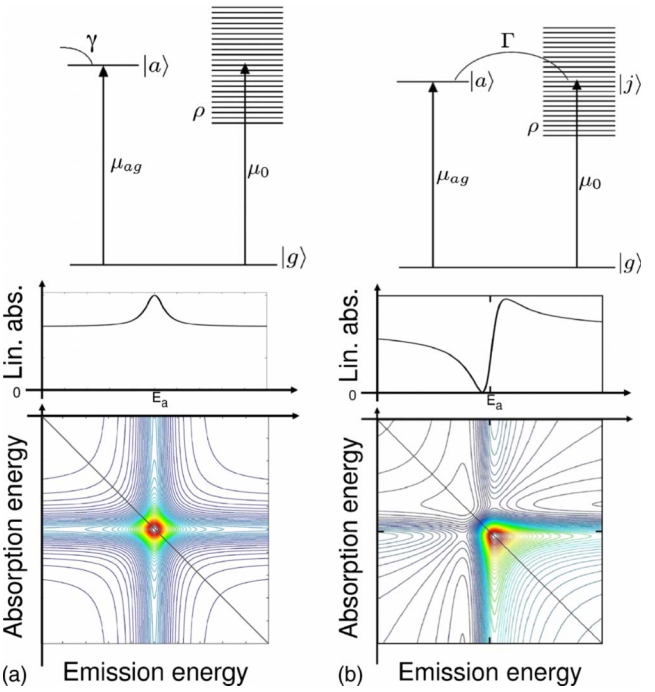

FIG. 4. (Color online) (a) From top to bottom: level scheme showing transition into a single state $|a\rangle$ with dipole matrix element μ_{ag} and phenomenological dephasing rate γ and into a continuum of states with matrix element μ_0; analytical results for the linear spectrum and amplitude 2DFTS, rephasing mode, corresponding to the level scheme above. (b) From top to bottom: level scheme showing transition into a single state $|a\rangle$ and into a continuum of states with matrix element μ_0, Γ is the coupling rate between $|a\rangle$ and the continuum; analytical results for the linear spectrum and amplitude 2DFTS, rephasing mode, corresponding to the level scheme above.

from the ground state to a single discrete state and a transition from this ground state into a continuum of states. In the classical scenario the optical transitions are given by an optical dipole matrix element μ_{ag} for transitions into the single discrete state and by a constant dipole matrix element μ_0 for those into the continuum, see Fig. 4. We here consider an unstructured continuum with a constant density of states ρ. However, the discrete state and the continuum are not considered to be eigenstates since there is coherent tunneling from the discrete excited state to the continuum states. The decay rate from the discrete resonance into the continuum is given by Γ. This scenario can be presented in form of a two-level system coupled to a continuum, see top of Fig. 4(b). The analytically calculated[17] linear spectrum in Fig. 4(b) illustrates the typical Fano character. The main reason for this Fano line shape is the interference of the transition into the discrete state and into the continuum of states. Thus once the coupling to the continuum is replaced by a phenomenological dephasing rate γ of the discrete transition, we obtain typical absorptive line of the discrete transition on top of continuum states [see the linear spectrum, Fig. 4(a)].

For the level system of Fig. 4(b) an analytical calculation of 2DFTS yields (see also Ref. 18)

$$P^{(3)}(\omega_t,\omega_\tau) = 2\frac{i\eta_0^3}{\hbar^3}\rho^2\mu_0^4\left(1+\frac{\frac{\Gamma}{2}(q-i)^2}{\frac{\Gamma}{2}-i(\hbar\omega_t-E_a)}\right)\times\left(1+\frac{\frac{\Gamma}{2}(q+i)^2}{\frac{\Gamma}{2}+i(\hbar\omega_\tau-E_a)}\right), \quad (5)$$

where

$$q=\left(\frac{2}{\pi\Gamma\rho}\right)^{1/2}\frac{\mu_{ag}}{\mu_0} \quad (6)$$

is the Fano parameter. Γ determines the purely homogeneous linewidth of the Fano line. The energy $\hbar\omega_t$ ($\hbar\omega_\tau$) is called emission (absorption) energy.

The 2DFTS shows the expected asymmetry and, more important, two prominent lines extending into the positive horizontal (emission energy) and into the negative vertical (absorption energy) directions, see bottom of Fig. 4(b). The width of the dominant peak (along the diagonal) is due to the homogeneous broadening induced by coupling to the continuum.

If we replace Γ by a phenomenological dephasing rate γ of the discrete transition [see top of Fig. 4(a)] we obtain symmetrical vertical and horizontal lines [bottom of Fig. 4(a)]. The resulting 2DFTS reflects the fact that there is the common ground state $|g\rangle$ for the discrete and continuum states.

B. Single exciton

Now we consider the real semiconductor and first focus on a single exciton in both the ordered and the disordered situations. Since we are interested in a contribution of disorder to the homogeneous broadening, we compare rephasing mode 2DFTS in the ordered and disordered situations.[16] It has to be noted that in this section we model disorder in such a way as to obtain pronounced disorder effects. In particular, the length scale of disorder has been chosen to be equal to Bohr radius which is about $2.4a$ and significant disorder amplitude, $W/J=0.1$ (corresponding to $W^v=0.334$ meV).

Figure 5 shows our results for Pauli-blocking calculations. In this case the nonlinear third-order signal includes the many-body interaction only in first order. Correlations in the $\chi^{(3)}$ limit also affect the line shape. These correlations are excluded. It allows us to extract the pure disorder-induced dephasing. Since the linear spectra provide solely the sum of homogeneous and inhomogeneous broadenings due to disorder (Fig. 5, upper figure), from the rephasing mode the homogeneous broadening can be extracted. Comparing Figs. 5(a) and 5(b) we obtain an additional disorder-induced homogeneous width of 0.22 meV. Note that in principle the imaginary-part 2DFTS [Fig. 5(b)] can provide even the spectral dependence of the disorder-induced dephasing, in other words, the lifetime of each localized exciton within the inhomogeneous ensemble. The arrows in Fig. 5(b) demonstrate

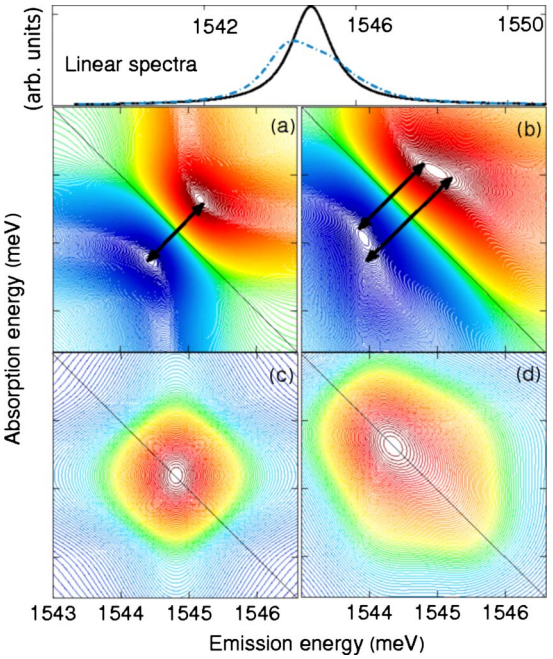

FIG. 5. (Color online) Upper figure: linear spectra for the ordered (solid line) and disordered (dot-dashed line) situation. Normalized imaginary-part 2DFTS, rephasing mode, (a) for the ordered and (b) for the disordered cases in the Pauli-blocking limit. Disorder amplitude of the heavy-hole exciton is 0.334 meV, corresponding to the disorder parameter $W/J=0.1$. The number of realizations is 40. Normalized amplitude for (c) ordered and (d) disordered cases, respectively. The energies at the vertical axis follow from reflection of the horizontal axis at the diagonal.

the increase in homogeneous broadening for higher energies within the inhomogeneous line.

We now compare the amplitude 2DFTS for the ordered and disordered [Fig. 5(c) and 5(d)] situations. In the disordered spectrum, we obtain a continuous decay along the diagonal toward higher energies. Toward lower energies, the decay is much faster, reflecting the asymmetric linear line shape of an exciton in a disordered environment. In addition to these features, which are already known from the linear spectrum, we notice a crosslike structure of the excitonic peak. Although such structure already appears for a single homogeneously broadened transition, Fig. 5(d). Here the extension toward both higher emission and absorption energy is more pronounced. This reflects the Fano-type coupling discussed above.

Thus, by using amplitude and imaginary-part 2DFTS rephasing mode both for the ordered and the disordered situations we are able to qualitatively identify couplings of discrete transitions to (disorder-modified) COM continua. There are two possible cases: (i) if the Fano-type scenario applies, we can interpret the mechanism leading to additional homogeneous broadening in terms of the coupling of a given localized exciton to the COM continuum of neighboring excitons. (ii) The alternative interpretation is not based on coupling between different neighboring excitons but applies already for a given exciton, where the lowest and dominant transition is optically coupled (via the ground state) to the COM continuum of the same exciton.

At present it is not possible to decide which of these two mechanisms applies to the given spectrum. In a Fano-type scenario one would expect to see a dip along the diagonal toward lower energies. However, for our present model we have a superposition of more than just one single excitonic peak due to the inhomogeneous broadening, which washes out this dip.

Finally, Fano-type couplings can also be induced by the many-particle interaction. For example, a light-hole excitonic peak "sits" on top of the continuum of a heavy-hole excitonic peak. Such kind of situation has been observed in the experiment and investigated in Refs. 31 and 32. Coupling between the light-hole exciton and the heavy-hole pair continuum due to the many-particle correlations was considered. Note that this particular coupling is be absent in the HF limit for the cocircular polarization of the excitation pulses. While the spectra calculated in the Pauli-blocking and HF approximations do not show the above-mentioned Fano signatures, they are clearly seen in the full calculation including the many-particle correlations and can therefore be classified as a many-body induced Fano effect.

VI. HEAVY- AND LIGHT-HOLE EXCITONS

We will consider in more detail the influence of disorder on heavy- and light-hole excitons by applying the full $\chi^{(3)}$ theory to the disordered situation. In contrast to Ref. 14, where we mimic disorder using a Gaussian convolution in order to illustrate the method, here, we model disorder microscopically. Therefore we are expecting that the heavy- and light-hole excitons have different inhomogeneous broadening, as was observed in the experiment. We emphasize that we now aim at a deeper understanding of experimental data at microscopic level if compared to the qualitative studies in the previous sections.

Analyzing experimental data, we conclude that the sample has weak disorder, this conclusion allows us to reduce the computational time thanks to a small number of realizations. The length scale of our correlated disorder is taken to be equal to the site separation a. The phenomenological dephasing times and effective masses are consistent with experimental data.

Our full calculations, which include also the correlations beyond HF, constitute even for a small number of realizations a major computational effort. We made initial calculations (not shown) in the Pauli-Blocking limit to make preliminary estimates of the phenomenological dephasing rates. Of course, for the realistic simulations we use the full calculations. The resulting homogeneous broadenings deviate from those of the Pauli-blocking calculations.

A. Heavy-hole exciton

We first compare the inhomogeneous broadenings of the heavy-hole exciton determined by the experiment [Fig. 6(a)] and by the numerical simulation [Fig. 6(b)], where the disorder is modeled as described in Sec. II.

At the top of Fig. 6 we show the linear spectra calculated using Gaussian convolution (solid line) and the linear spectrum for the microscopically modeled disorder (dashed-dotted line). We are able to fit the linear spectrum using Gaussian convolution. On the other hand, for disordered semiconductors it is not possible to fit the line shape of 2DFTS by this method since it contains more spectral information than the linear spectrum.

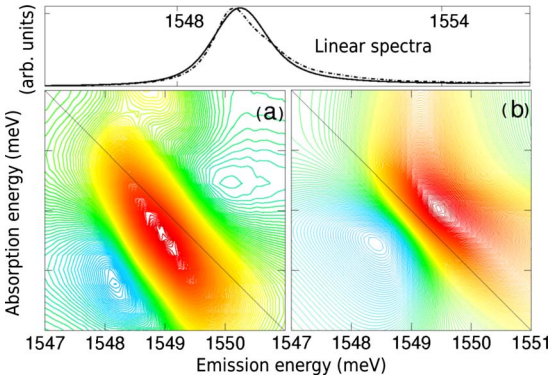

FIG. 6. (Color online) Upper figure: normalized linear spectra for the ordered (solid line) and disordered (dot-dashed line) situation at the heavy-hole excitonic peak. Normalized imaginary-part 2DFTS rephasing mode: (a) experimental data are taken from Ref. 14 and (b) modeled disorder with the amplitude of 0.72 meV, $W/J=0.4$, and the number of realizations is 13. Disorder length scale $L=a$. The energies at the vertical axis follow from reflection of the horizontal axis at the diagonal.

We apply the method, which was described in Ref. 16 in order to determine the homogeneous and inhomogeneous broadenings. From the dispersive (either in the real- or the imaginary-part spectra) rephasing mode spectra we determine Ω^{hom}, which is proportional to the total homogeneous width, by measuring the energetic distance between the maximum and the minimum at a line perpendicular to the diagonal. The sum of inhomogeneous and homogeneous widths follows in a similar way from the nonrephasing spectra. The extracted values are shown in Fig. 7 (black square: experiment and black triangle: simulation). It shows that the amplitude of the disorder in our simulation can be well estimated and implemented in our simulations, also the phenomenological dephasing time can be fitted to the experiment. Thus the black triangle error bars for homogeneous and inhomogeneous broadenings of the heavy-hole exciton obtained from the present calculation show good agreement with the experimental ones (black square).

We focus on the line shape of 2DFTS, rephasing mode. The line shape of the experimental imaginary-part 2DFTS rephasing mode [Fig. 6(a)] shows slightly absorptive character instead of dispersive one in the simulations [Fig. 6(b)]. The reason could be the not sufficiently controlled global phase in the experiment, which can invert imaginary into real part.[33] Of course, it cannot be excluded that the schematic nature of our present model leads to this slight discrepancy. The distance between minimum and maximum does not increase due to Fano effect as demonstrated in the previous section. That means that homogeneous broadening is almost not influenced by disorder because we here have the case of weak disorder ($L<a_B$). The butterfly form of the imaginary part shown in Fig. 5(b) cannot be identified in Fig. 6. Note

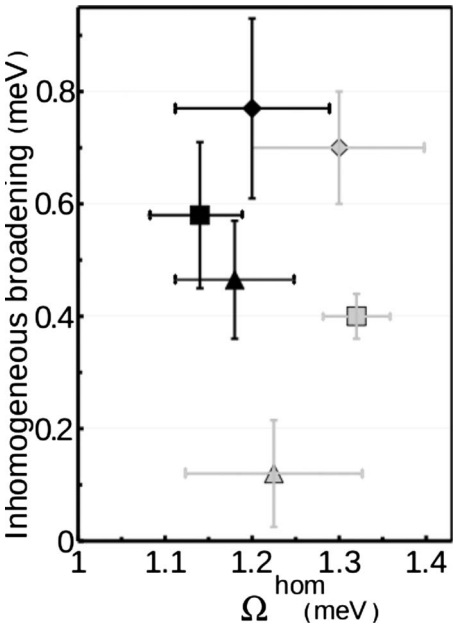

FIG. 7. Inhomogeneous broadening of the excitons (black identifies heavy-hole exciton and gray the light-hole exciton) vs Ω^{hom}, extracted from the 2DFTS, rephasing mode. The squares show experimental data for GaAs/AlGaAs taken from (Ref. 14), diamonds are the data of the ordered 2DFTS, which have been broadened by Gaussian with the FWHM of 0.72 meV, and triangles are the data extracted from the present calculation. We used the following disordered parameters: $W/J=0.4$, $W^h=0.72$ meV, $W^l=0.9$ meV, the number of realizations is 13, and disorder length scale $L=a$. Estimated error bars are shown.

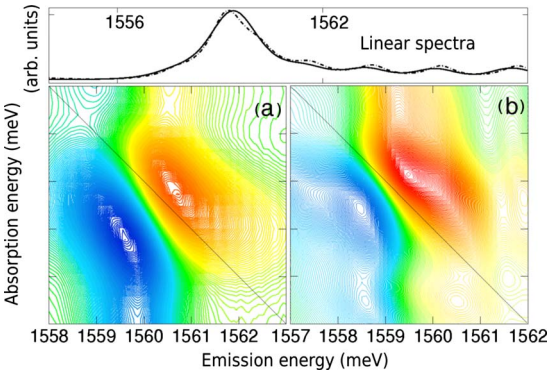

FIG. 8. (Color online) Upper figure: normalized linear spectra for the ordered (solid line) and disordered (dot-dashed line) situation at the light-hole excitonic peak. Normalized imaginary-part 2DFTS rephasing mode: (a) experimental data are taken from Ref. 14 and (b) modeled disorder with the amplitude of 0.9 meV, $W/J=0.4$, and number of realizations is 13. Disorder length scale $L=a$. The energies at the vertical axis follow from reflection of the horizontal axis at the diagonal.

that in the above-mentioned example [Fig. 5(b)] we have chosen our model parameter in order to obtain strong disorder effects ($L=a_B$).

Using the nonrephasing mode (not shown here) we extract the inhomogeneous broadening of the simulated spectrum, which is smaller by 35% compared to the input disorder amplitude used in the calculations (see Fig. 7, compare the black triangle with corresponding $W^h=0.72$ meV). The explanation of the reduced inhomogeneous broadening is the averaging effect, which is in particularly effective since the Bohr radius of the heavy-hole exciton is larger than the length scale of the disorder. This reduction also agrees with the dependence of the FWHM on J^v shown in Fig. 3 for $J^v=1.8$ meV (crosses indicate FWHM for the h heavy- and l light-hole excitons, respectively). Our material parameters correspond almost to the minimum of the curvature, i.e., the crossover between the two regimes.

B. Light-hole exciton

Now we focus on the light-hole exciton. In the experimental samples the light-hole exciton is energetically on top of the pair continuum of the heavy-hole exciton. For the cocircular excitation considered here, these two sets of transitions only couple due to many-particle correlations. In the full calculations, we therefore expect that homogeneous and, in particular, inhomogeneous broadenings are influenced by this mechanism. Note that the phenomenological dephasing time for the light-hole exciton is somewhat overestimated [Fig. 7 (compare the gray square and triangle along the X axis)]. As it was mentioned at the beginning of this section, preliminary calculations on the Pauli-blocking level have been made in order to get an estimate for the phenomenological dephasing time. This was working well for the heavy-hole exciton. Due to strong coupling of the light-hole exciton to the pair continuum of the heavy-hole exciton the homogeneous broadening of the light-hole exciton has been overestimated. However, the second reason for the increase in the homogeneous broadening could be disorder. As the amplitude of the disorder scales with the inverse mass of the light hole, for the $W/J=0.4$ we obtain a larger $W^l=0.9$ meV than for the heavy-hole exciton, which is $W^h=0.72$ meV. Thus we expect stronger influence of disorder on the light-hole exciton.

Figure 8 shows the linear spectra of the light-hole exciton (at the top) and the imaginary part of the rephasing mode 2DFTS. In comparison to the experiment [Fig. 8(a)] our numerical simulations (b) reproduce the butterfly form of the dispersive feature quite well. The Gaussian convolution leads to simple elongation along the diagonal.[14] In reality the ovals of the maximum and minimum at the higher frequencies reorientate horizontally and vertically, respectively. This is due to the Fano effect, which is induced by both the light-hole exciton coupling to the heavy-hole pair continuum and by the coupling to its own center-of-mass continuum. In order to distinguish these two mechanisms one could carry out Pauli-blocking simulations because the first mechanism on this level is absent in the cocircular excitation scenario. Nevertheless the homogeneous broadening extracted from the rephasing mode spectrum is only about 2% larger than our input parameter (the error bars have not been taken into account), see Fig. 7, gray triangle. Thus, we conclude that for the present model disorder-induced dephasing is not easy to be identified.

We now concentrate on inhomogeneous broadening. As we learned from the heavy-hole exciton investigations the

inhomogeneous broadening is influenced by material parameters such as effective mass and also (see first part of the paper) by the disorder length scale. Since we consider here a minimal length scale of disorder to be equal to the site separation a, we focus on the effective mass. In the experiment, the effective mass for the light-hole exciton has been observed to be smaller than for the heavy-hole exciton. Strain could be a possible reason for this ratio of masses. We perform our simulations using the same trend.

Applying our method for the determination of the inhomogeneous broadening, we obtain an almost eight times smaller value if compared to the amplitude of disorder W^l. From Fig. 3 we see that the reason cannot be the different masses of the holes, which lead to such large reduction in the inhomogeneous width. The main difference in the present simulations compared to those leading to Fig. 3 is twofold: (i) the present calculation treats nonlinear spectrum and (ii) the light-hole exciton sits on the top of the heavy-hole pair continuum. Since these transitions are coupled due to correlations, we conclude, that the reduction in the inhomogeneous width of the light-hole exciton is due to this coupling. Continuum states, here the heavy-hole pair continuum, are generally less affected by disorder than discrete states like the exciton. We conclude that this insensitivity of the continuum states is transferred to the light-hole exciton by many-particle correlations. Note that here we are discussing the inhomogeneous width of a nonlinear spectrum, which cannot be expected to be equal to that of a linear spectrum.

Using Gaussian convolution, the homogeneous and inhomogeneous broadenings of both excitons are not distinguishable (black and gray diamonds in Fig. 7) since the error boxes cross. It has to be remarked that using Gaussian convolution the averaging processes cannot be modeled. Thus, satisfactory agreement with experimental data can only be expected by microscopically modeling the disorder potential.

VII. CONCLUSION

A case study has been performed on the basis of a one-dimensional tight-binding model which illustrates the influence of weak disorder, characterized by various length scales, on homogeneous and inhomogeneous excitonic line broadenings. Nonlinear spectra have been studied, in particular, that allow one to determine homogeneous and inhomogeneous contributions to the linewidth separately. For a length scale smaller than exciton Bohr radius, both contributions are influenced by averaging due to the relative motion of the electron-hole pair. This averaging reduces the effective disorder amplitude. Additional disorder-induced homogeneous width is due to coupling to center-of-mass excitonic continua, where Fano-type couplings can play a role.

By applying our model to existing experimental data, we found that many-particle correlations can lead to contributions to the inhomogeneous width. In the situation of the experiment it has been shown that this coupling can dramatically reduce the inhomogeneous width if one set of transitions is a continuum.

In the nonlinear regime, in addition to excitonic transitions, also features induced by Coulomb correlations appear close to the energetic position of the excitonic transition.[19] These include resonances due to bound biexcitons energetically slightly below the excitonic peak and induced absorption due to states of unbound two-exciton transitions slightly above the exciton. These additional features tend to obscure the disorder-related effects. While a calculation in the Pauli-blocking limit can concentrate on pure disorder-induced effects this is not possible in reality. In order to reduce these correlation-induced features in an experiment, suitable polarizations of the three excitation pulses in the FWM (2DFTS) scheme have to be chosen. The selection rules[34] predict that for cross circular (right handed and left handed), for colinear and, in particular, for cross-linear polarized pulses bound biexcitonic features are strong while for cocircular polarization bound biexcitons are absent in the nonlinear response. We therefore suggest to study 2DFTS for a cocircular polarization scheme on quantum wells, which are fabricated in such a way that various length scales of the disorder can be assumed to exist. For nominally equal amplitude of the disorder potential, which depends on the average well width, various length scales of the well-width fluctuation can be induced by suitable growth conditions.[35] The largest disorder effects on the homogeneous broadening, i.e., the Fano-induced features, are predicted for a length scale that is close to the exciton Bohr radius.

ACKNOWLEDGMENTS

This work has been supported by the DFG through the Emmy Noether Program Grant No. FO 637/1-1 and the DFG Research Training Group GRK 1464, and by the John-von-Neumann Institute für Computing (NIC), Jülich, Germany.

[1] A. Thränhardt, S. Kuckenburg, A. Knorr, P. Thomas, and S. W. Koch, Phys. Rev. B **62**, 16802 (2000).
[2] R. Zimmermann (private communication).
[3] S. Abe and Y. Toyozawa, J. Phys. Soc. Jpn. **50**, 2185 (1981).
[4] S. D. Baranovskii and A. L. Efros, Sov. Phys. Semicond. **12**, 1328 (1978).
[5] S. D. Baranovskii, U. Doerr, P. Thomas, A. Naumov, and W. Gebhardt, Phys. Rev. B **48**, 17149 (1993).
[6] R. Zimmermann and E. Runge, J. Lumin. **60-61**, 320 (1994).
[7] R. Zimmermann, F. Große, and E. Runge, Pure Appl. Chem. **69**, 1179 (1997).
[8] *Optical Properties of Condensed Matter and Applications*, edited by J. Singh (Wiley, New York, 2006).
[9] C. Sieh, T. Meier, A. Knorr, F. Jahnke, P. Thomas, and S. W. Koch, Eur. Phys. J. B **11**, 407 (1999).
[10] S. Weiser, T. Meier, J. Möbius, A. Euteneuer, E. J. Mayer, W. Stolz, M. Hofmann, W. W. Rühle, P. Thomas, and S. W. Koch, Phys. Rev. B **61**, 13088 (2000).

[11] Ch. Lonsky, P. Thomas, and A. Weller, Phys. Rev. Lett. **63**, 652 (1989).
[12] D. Brinkmann, Ph.D. thesis, Philipps University, Marburg, 1998.
[13] M. Cho, Chem. Rev. **108**, 1331 (2008).
[14] I. Kuznetsova, T. Meier, S. T. Cundiff, and P. Thomas, Phys. Status Solidi C **6**, 445 (2009).
[15] T. Meier, P. Thomas, and S. W. Koch, *Coherent Semiconductor Optics-From Basic Concepts to Nanostructure Applications* (Springer, Berlin, 2007).
[16] I. Kuznetsova, T. Meier, S. T. Cundiff, and P. Thomas, Phys. Rev. B **76**, 153301 (2007).
[17] U. Fano, Phys. Rev. **124**, 1866 (1961).
[18] T. Meier, A. Schulze, P. Thomas, H. Vaupel, and K. Maschke, Phys. Rev. B **51**, 13977 (1995).
[19] I. Kuznetsova, P. Thomas, T. Meier, T. Zhang, X. Li, R. P. Mirin, and S. T. Cundiff, Solid State Commun. **142**, 154 (2007).
[20] L. Bányai, I. Galbraith, C. Ell, and H. Haug, Phys. Rev. B **36**, 6099 (1987).
[21] S. T. Cundiff, Opt. Express **16**, 4639 (2008).
[22] L. Yang, I. V. Schweigert, S. T. Cundiff, and S. Mukamel, Phys. Rev. B **75**, 125302 (2007).
[23] L. Yang and S. Mukamel, Phys. Rev. Lett. **100**, 057402 (2008).
[24] R. J. Elliott, Phys. Rev. **108**, 1384 (1957).
[25] V. M. Axt and A. Stahl, Z. Phys. B: Condens. Matter **93**, 195 (1994).
[26] F. Urbach, Phys. Rev. **92**, 1324 (1953).
[27] M. V. Kurik, Phys. Status Solidi A **8**, 9 (1971).
[28] F. Jahnke, M. Koch, T. Meier, J. Feldmann, W. Schäfer, P. Thomas, S. W. Koch, E. O. Göbel, and H. Nickel, Phys. Rev. B **50**, 8114 (1994).
[29] T. Zhang, Ph.D. thesis, JILA, 2008.
[30] T. Zhang, C. N. Borca, X. Li, and S. T. Cundiff, Opt. Express **13**, 7432 (2005).
[31] C. N. Borca, T. H. Zhang, X. Li, and S. T. Cundiff, Chem. Phys. Lett. **416**, 311 (2005).
[32] I. Kuznetsova, P. Thomas, T. Meier, T. Zhang, and S. T. Cundiff, Conference Digest of CLEO/Europe-IQEC, 2007.
[33] I. Kuznetsova, Ph.D. thesis, Philipps University, Marburg, 2007.
[34] M. Lindberg, R. Binder, Y. Z. Hu, and S. W. Koch, Phys. Rev. B **49**, 16942 (1994).
[35] M. A. Herman, D. Bimberg, and J. Christen, J. Appl. Phys. **70**, R1 (1991).